Journal of Computational Mathematics, Vol.22, No.2, 2004, 250–274.

LOCAL DISCONTINUOUS GALERKIN METHODS FOR THREE CLASSES OF NONLINEAR WAVE EQUATIONS *[1)]

Yan Xu
(*Department of Mathematics, University of Science and Technology of China, Hefei 230026, China*)
(*E-mail: yxu1@mail.ustc.edu.cn*)

Chi-wang Shu
(*Division of Applied Mathematics, Brown University, Providence, RI 02912, USA*)
(*E-mail: shu@dam.brown.edu*)

Dedicated to Professor Zhong-ci Shi on the occasion of his 70th birthday

Abstract

In this paper, we further develop the local discontinuous Galerkin method to solve three classes of nonlinear wave equations formulated by the general KdV-Burgers type equations, the general fifth-order KdV type equations and the fully nonlinear $K(n,n,n)$ equations, and prove their stability for these general classes of nonlinear equations. The schemes we present extend the previous work of Yan and Shu [30, 31] and of Levy, Shu and Yan [24] on local discontinuous Galerkin method solving partial differential equations with higher spatial derivatives. Numerical examples for nonlinear problems are shown to illustrate the accuracy and capability of the methods. The numerical experiments include stationary solitons, soliton interactions and oscillatory solitary wave solutions. The numerical experiments also include the compacton solutions of a generalized fifth-order KdV equation in which the highest order derivative term is nonlinear and the fully nonlinear $K(n,n,n)$ equations.

Mathematics subject classification: 65M60, 35Q53
Key words: Local discontinuous Galerkin method, KdV-Burgers equation, Fifth-order KdV equation, Stability.

1. Introduction

In this paper we further develop the local discontinuous Galerkin method to solve three classes of generalized nonlinear wave equations formulated by the KdV-Burgers type (KdVB) equations

$$u_t + f(u)_x - (a(u)u_x)_x + (r'(u)g(r(u)_x)_x)_x = 0, \tag{1.1}$$

the fifth-order KdV type equations

$$u_t + f(u)_x + (r'(u)g(r(u)_x)_x)_x + (s'(u)h(s(u)_{xx})_{xx})_x = 0, \tag{1.2}$$

and the fifth-order fully nonlinear $K(n,n,n)$ equations

$$u_t + (u^n)_x + (u^n)_{xxx} + (u^n)_{xxxxx} = 0 \tag{1.3}$$

* Received January 31, 2004.
[1)] The research of this author is supported by NNSFC grant 10028103 while he is in residence at the Department of Mathematics, University of Science and Technology of China, Hefei 230026, China. Additional support is provided by ARO grant DAAD19-00-1-0405 and NSF grant DMS-0207451.

where $f(u)$, $a(u) \geq 0$, $r(u)$, $s(u)$, $g(p)$ and $h(q)$ are arbitrary (smooth) nonlinear functions. The schemes we present extend the previous work of Yan and Shu [30, 31] and of Levy, Shu and Yan [24] on local discontinuous Galerkin method solving partial differential equations with higher spatial derivatives.

A special case of equation (1.1) is the KdV-Burgers equation

$$u_t + \varepsilon u u_x - \alpha u_{xx} + \beta u_{xxx} = 0 \tag{1.4}$$

derived by Su and Gardner [28], which is a model for nonlinear wave motion incorporating several important physical phenomena, namely dispersion, nonlinear advection and viscosity. The equation arises in the description of long wave propagation in shallow water [2] and in weakly nonlinear plasma physics with dissipation [18]. Efforts to shed light on this problem by means of numerical experiments are made in [3, 6, 33] and the references therein.

The fifth order nonlinear evolution equation

$$u_t + u u_x + u_{xxx} - \delta u_{xxxxx} = 0, \tag{1.5}$$

which is a special case of (1.2), is known as the critical surface-tension model [19]. This equation arises in the modeling of weakly nonlinear waves in a wide variety of media, including magneto-acoustic waves in plasma [23] and long waves in the liquids under ice sheets [25]. There are only a few numerical works in the literature to solve the fifth-order KdV equation. A general type of "semi-localized" solitary wave solutions has been investigated by Kawahara [23], which gave the first numerical evidence of oscillatory solitary wave solutions. Numerical experiments on the semi-localized solutions and their interactions appeared in [4, 5]. In recent numerical studies of break-up of initial data, Hyman and Rosenau [21] have observed a variety of localized pulsating "multiplet" solutions.

The fifth-order fully nonlinear $K(n, n, n)$ equations (1.3) are useful for describing the dynamics of various physical systems. Such nonlinearly dispersive partial differential equations support compacton solutions. A variety of explicit compact solitary wave structures of these fifth-order nonlinear dispersive equations are constructed in [16, 26]. The numerical simulations of these equations in [26] have also revealed the existence of compact traveling breathers. Recently, some attempts have been made to numerically study the stability of the compacton solutions of the fifth-order nonlinear dispersive equations in [15]. The lack of smoothness at the edge of compacton introduces high-frequency dispersive errors into the calculation. It is a challenge to design stable and accurate numerical schemes for solving equation (1.3).

The discontinuous Galerkin method we discuss in this paper is a class of finite element methods using completely discontinuous piecewise polynomial space for the numerical solution and the test functions in the spatial variables, coupled with explicit and nonlinearly stable high order Runge-Kutta time discretization [27]. It was first developed for hyperbolic conservation laws containing first derivatives by Cockburn et al. in a series of papers [11, 10, 8, 12]. For a detailed description of the method as well as its implementation and applications, we refer the readers to the lecture notes [7], the survey paper [9], other papers in that Springer volume, and the review paper [14].

These discontinuous Galerkin methods were generalized to solve a convection diffusion equation (containing second derivatives) by Cockburn and Shu [13]. Their work was motivated by the successful numerical experiments of Bassi and Rebay [1] for the compressible Navier-Stokes equations. Later, Yan and Shu developed a local discontinuous Galerkin method for a general KdV type equation containing third derivatives in [30] and generalized the local discontinuous Galerkin method to PDEs with fourth and fifth spatial derivatives in [31]. Recently, Levy, Shu and Yan [24] developed local discontinuous Galerkin methods for solving nonlinear dispersive equations that have compactly supported traveling wave solutions, the so-called "compactons".

The schemes we present in this paper extend the work of Yan and Shu [30, 31] and of Levy, Shu and Yan [24]. The paper is organized as follows. In section 2 we present local discontinuous

Galerkin methods for three classes of general nonlinear wave equations. In section 2.1, we present the methods for the KdVB type nonlinear problems. We also present a theoretical result of L^2 stability for the nonlinear case as well as an error estimate for the linear case. In section 2.2, we present and analyze the local discontinuous Galerkin methods for the fifth-order KdV type nonlinear problems and give a proof of the nonlinear L^2 stability. In section 2.3, we present a local discontinuous Galerkin method for the nonlinear fifth order $K(n,n,n)$ equations and prove its L^{n+1} stability for odd n. Section 3 contains numerical results for the nonlinear problems to demonstrate the accuracy and capability of the methods. In section 3.1, both KdV type and KdVB type solutions are simulated. In section 3.2, the numerical experiments for the fifth-order KdV equations containing stationary solitons, soliton interactions and oscillatory solitary wave solutions are presented. In section 3.3, we present numerical results of a generalized fifth-order KdV equation in which the highest order derivative term is nonlinear. In section 3.4, we show the accuracy test results and compacton solutions of the $K(n,n,n)$ equations for $n=3$ and $n=5$. Concluding remarks are included in section 4.

2. The Local Discontinuous Galerkin Method for Nonlinear Wave Equations

In this section, we present and analyze local discontinuous Galerkin methods for three classes of general nonlinear wave equations.

2.1. KdVB type equations

We first present and analyze the local discontinuous Galerkin method for the following KdVB type nonlinear problems:

$$u_t + f(u)_x - (a(u)u_x)_x + (r'(u)g(r(u)_x)_x)_x = 0 \tag{2.1}$$

with an initial condition

$$u(x,0) = u_0(x) \tag{2.2}$$

and periodic boundary conditions. Here $f(u)$, $a(u) \geq 0$, $r(u)$ and $g(q)$ are arbitrary (smooth) nonlinear functions. Notice that the assumption of periodic boundary conditions is for simplicity only and is not essential: the method can be easily designed for non-periodic boundary conditions and such non-periodic boundary conditions are used in the numerical experiments in next section. Equation (2.1) without the third dissipation term was considered in [30] and [24].

We denote the mesh by $I_j = [x_{j-\frac{1}{2}}, x_{j+\frac{1}{2}}]$, for $j = 1, \ldots, N$. The center of the cell is $x_j = (x_{j-\frac{1}{2}} + x_{j+\frac{1}{2}})/2$ and $\Delta x_j = x_{j+\frac{1}{2}} - x_{j-\frac{1}{2}}$. We denote by $u^+_{j+\frac{1}{2}}$ and $u^-_{j+\frac{1}{2}}$ the values of u at $x_{j+\frac{1}{2}}$, from the right cell I_{j+1}, and from the left cell I_j, respectively. We define the piecewise-polynomial space $V_{\Delta x}$ as the space of polynomials of degree up to k in each cell I_j, i.e.

$$V_{\Delta x} = \{v : \quad v \in P^k(I_j) \quad \text{for } x \in I_j, \quad j = 1, \ldots, N\}. \tag{2.3}$$

To simplify the notation, we still use u to denote the numerical solution.

To define the local discontinuous Galerkin method, we rewrite the equation (2.1) as a first order system:

$$\begin{aligned} u_t + f(u)_x - (b(u)v)_x + (r'(u)p)_x = 0, \\ v - B(u)_x = 0, \quad p - g(q)_x = 0, \quad q - r(u)_x = 0 \end{aligned} \tag{2.4}$$

where $b(u) = \sqrt{a(u)}$ and $B(u) = \int^u b(\tau)d\tau$. We can use the discontinuous Galerkin method to solve (2.4), resulting in the following scheme: find $u, p, v, q \in V_{\Delta x}$ such that, for all test functions $\rho, \psi, \phi, \varphi \in V_{\Delta x}$,

$$\int_{I_j} u_t \rho dx - \int_{I_j} (f(u) - b(u)v + r'(u)p)\rho_x dx + (\hat{f} - \hat{b}\hat{v} + \hat{r'}\hat{p})_{j+\frac{1}{2}}\rho^-_{j+\frac{1}{2}} - (\hat{f} - \hat{b}\hat{v} + \hat{r'}\hat{p})_{j-\frac{1}{2}}\rho^+_{j-\frac{1}{2}} = 0$$

$$\int_{I_j} v\psi dx + \int_{I_j} B(u)\psi_x dx - \hat{B}_{j+\frac{1}{2}}\psi^-_{j+\frac{1}{2}} + \hat{B}_{j-\frac{1}{2}}\psi^+_{j-\frac{1}{2}} = 0 \tag{2.5}$$

$$\int_{I_j} p\phi dx + \int_{I_j} g(q)\phi_x dx - \hat{g}_{j+\frac{1}{2}}\phi^-_{j+\frac{1}{2}} + \hat{g}_{j-\frac{1}{2}}\phi^+_{j-\frac{1}{2}} = 0$$

$$\int_{I_j} q\varphi dx + \int_{I_j} r(u)\varphi_x dx - \hat{r}_{j+\frac{1}{2}}\varphi^-_{j+\frac{1}{2}} + \hat{r}_{j-\frac{1}{2}}\varphi^+_{j-\frac{1}{2}} = 0$$

The "hat" terms in (2.5) are the boundary terms that emerge from integration by parts. These are the so-called "numerical fluxes" which should be designed based on different guiding principles for different PDEs to ensure stability. It turns out that we can take the simple choices such that

$$\hat{f} = \hat{f}(u^-, u^+), \quad \hat{g} = \hat{g}(q^-, q^+), \quad \hat{b} = \frac{B(u^+) - B(u^-)}{u^+ - u^-}, \quad \hat{r'} = \frac{r(u^+) - r(u^-)}{u^+ - u^-}$$

$$\hat{B} = B(u^-), \quad \hat{v} = v^+, \quad \hat{r} = r(u^-), \quad \hat{p} = p^+ \tag{2.6}$$

where we have omitted the half-integer indices $j + \frac{1}{2}$ as all quantities in (2.6) are computed at the same points (i.e. the interfaces between the cells). Here $\hat{f}(u^-, u^+)$ and $-\hat{g}(q^-, q^+)$ are monotone fluxes, i.e. Lipschitz continuous in both arguments, consistent (i.e. $\hat{f}(u, u) = f(u)$), non-decreasing in the first argument and non-increasing in the second argument. Examples of monotone fluxes which are suitable for discontinuous Galerkin methods can be found in, e.g., [11]. We could for example use the simple Lax-Friedrichs flux

$$\hat{f}(u^-, u^+) = \frac{1}{2}(f(u^-) + f(u^+) - \alpha(u^+ - u^-)), \quad \alpha = \max|f'(u)|$$

where the maximum is taken over a relevant range of u; This flux is used in the numerical experiments in next section. The algorithm is now well defined.

We remark that the choice for the fluxes (2.6) is not unique. In fact the crucial part is taking $\hat{p}$ and $\hat{r}$ from opposite sides and taking $\hat{v}$ and $\hat{B}$ from opposite sides.

With such a choice of fluxes we can get the theoretical results of L^2 stability for the general nonlinear case and an error estimate for the linear case.

Proposition 2.1 (cell entropy inequality). *There exist numerical entropy fluxes $\hat{\Phi}_{j+\frac{1}{2}}$ such that the solution to the scheme (2.5) - (2.6) satisfies*

$$\frac{1}{2}\frac{d}{dt}\int_{I_j} u^2(x,t)dx + \hat{\Phi}_{j+\frac{1}{2}} - \hat{\Phi}_{j-\frac{1}{2}} \leq 0.$$

Summing up the cell entropy inequalities, we obtain

Corollary 2.2 (L^2 stability). *The solution to the scheme (2.5) - (2.6) satisfies the L^2 stability*

$$\frac{d}{dt}\int_0^L u^2(x,t)dx \leq 0.$$

The stability result obtained here can be used to get an error estimate in L^2 for the numerical solution u when the equation (2.1) is linear. Without loss of generality we can consider the error estimate for linearized KdVB equation

$$u^e_t + u^e_x - \alpha u^e_{xx} + \beta u^e_{xxx} = 0 \tag{2.7}$$

where we use u^e to denote the exact solution to equation (2.7) since u is used to denote the numerical solution.

Proposition 2.3 (error estimate). *The error for the scheme (2.5) - (2.6) applied to the linearized KdVB equation (2.7) satisfies*

$$\|u^e - u\|_0 \leq C\|u^e\|_{k+1}\Delta x^{k+\frac{1}{2}} \tag{2.8}$$

where $||\cdot||_m$ is the standard Sobolev m norm and the constant C depends on the time t.

Propositions 2.1 and 2.3 can be proven by the standard techniques of proving the L^2-stability and convergence of the semidiscrete discontinuous Galerkin methods, see for example [13] and [30]. We will thus not give the details here.

2.2. Fifth-order KdV type equations

In this section, we present and analyze the local discontinuous Galerkin method for the following fifth order nonlinear problem:

$$u_t + f(u)_x + (r'(u)g(r(u)_x)_x + (s'(u)h(s(u)_{xx})_{xx})_x = 0, \tag{2.9}$$

with an initial condition

$$u(x,0) = u_0(x)$$

and periodic boundary conditions. Here $f(u)$, $r(u)$, $s(u)$, $g(p)$ and $h(q)$ are arbitrary (smooth) nonlinear functions. Equation (2.9) is more general that those considered in [31].

To define the local discontinuous Galerkin method, we rewrite the equation (2.9) as a first order system:

$$\begin{aligned} &u_t + f(u)_x + (r'(u)p)_x + (s'(u)v)_x = 0 \\ &p - g(q)_x = 0, \quad q - r(u)_x = 0, \quad v - w_x = 0 \\ &w - h(l)_x = 0, \quad l - z_x = 0, \quad z - s(u)_x = 0 \end{aligned} \tag{2.10}$$

We can use the discontinuous Galerkin method to solve (2.10), resulting the following scheme: find $u, p, q, v, w, l, z \in V_{\Delta x}$ such that, for all test functions $\rho, \phi, \varphi, \psi, \eta, \xi, \zeta \in V_{\Delta x}$,

$$\int_{I_j} u_t\rho dx - \int_{I_j} (f(u)+r'(u)p+s'(u)v)\rho_x dx + (\hat{f}+\hat{r'}\hat{p}+\hat{s'}\hat{v})_{j+\frac{1}{2}}\rho^-_{j+\frac{1}{2}} - (\hat{f}+\hat{r'}\hat{p}+\hat{s'}\hat{v})_{j-\frac{1}{2}}\rho^+_{j-\frac{1}{2}} = 0$$

$$\begin{aligned} &\int_{I_j} p\phi dx + \int_{I_j} g(q)\phi_x dx - \hat{g}_{j+\frac{1}{2}}\phi^-_{j+\frac{1}{2}} + \hat{g}_{j-\frac{1}{2}}\phi^+_{j-\frac{1}{2}} = 0 \\ &\int_{I_j} q\varphi dx + \int_{I_j} r(u)\varphi_x dx - \hat{r}_{j+\frac{1}{2}}\varphi^-_{j+\frac{1}{2}} + \hat{r}_{j-\frac{1}{2}}\varphi^+_{j-\frac{1}{2}} = 0 \\ &\int_{I_j} v\psi dx + \int_{I_j} w\psi_x dx - \hat{w}_{j+\frac{1}{2}}\psi^-_{j+\frac{1}{2}} + \hat{w}_{j-\frac{1}{2}}\psi^+_{j-\frac{1}{2}} = 0 \\ &\int_{I_j} w\eta dx + \int_{I_j} h(l)\eta_x dx - \hat{h}_{j+\frac{1}{2}}\eta^-_{j+\frac{1}{2}} + \hat{h}_{j-\frac{1}{2}}\eta^+_{j-\frac{1}{2}} = 0 \\ &\int_{I_j} l\xi dx + \int_{I_j} z\xi_x dx - \hat{z}_{j+\frac{1}{2}}\xi^-_{j+\frac{1}{2}} + \hat{z}_{j-\frac{1}{2}}\xi^+_{j-\frac{1}{2}} = 0 \\ &\int_{I_j} z\zeta dx + \int_{I_j} s(u)\zeta_x dx - \hat{s}_{j+\frac{1}{2}}\zeta^-_{j+\frac{1}{2}} + \hat{s}_{j-\frac{1}{2}}\zeta^+_{j-\frac{1}{2}} = 0. \end{aligned} \tag{2.11}$$

We can again take the following simple choices of fluxes to guarantee stability:

$$\hat{f} = \hat{f}(u^-, u^+), \quad \hat{g} = \hat{g}(q^-, q^+), \quad \hat{h} = \hat{h}(l^-, l^+),$$

$$\hat{r'} = \frac{r(u^+) - r(u^-)}{u^+ - u^-}, \quad \hat{s'} = \frac{s(u^+) - s(u^-)}{u^+ - u^-} \tag{2.12}$$
$$\hat{p} = p^+, \quad \hat{r} = r(u^-), \quad \hat{v} = v^+, \quad \hat{s} = s(u^-), \quad \hat{w} = w^+, \quad \hat{z} = z^-,$$

where we have again omitted the half-integer indices $j + \frac{1}{2}$. Here $\hat{f}(u^-, u^+)$, $-\hat{g}(q^-, q^+)$ and $\hat{h}(l^-, l^+)$ are monotone fluxes. The algorithm is now well defined.

We remark that the choice for the fluxes (2.12) is not unique. In fact the crucial part is taking $\hat{p}$ and $\hat{r}$ from opposite sides, $\hat{v}$ and $\hat{z}$ from opposite sides, and $\hat{w}$ and $\hat{z}$ from opposite sides.

With such a choice of fluxes we have

Proposition 2.4 (L^2 stability). *The solution to the scheme (2.11) - (2.12) satisfies the L^2 stability*

$$\frac{d}{dt}\int_0^L u^2(x,t)dx \le 0.$$

Proof. Since (2.11) holds for any test functions in $V_{\Delta x}$, we can choose

$$\rho = u, \quad \phi = q, \quad \varphi = -p, \quad \psi = z, \quad \eta = -l, \quad \xi = w, \quad \zeta = -v.$$

With these choices of test functions and summing up the seven equations in (2.11) we obtain

$$\int_{I_j} u_t u dx + \hat{\Phi}_{j+\frac{1}{2}} - \hat{\Phi}_{j-\frac{1}{2}} + \Theta_{j-\frac{1}{2}} = 0$$

where the numerical entropy flux is given by

$$\hat{\Phi} = -F(u^-) + G(q^-) - H(l^-) + (\hat{f} + \hat{r'}\hat{p} + \hat{s'}\hat{v})u^- - \hat{g}q^- + \hat{h}l^-$$
$$+w^-z^- - \hat{z}w^- - \hat{w}z^- - r(u^-)p^- + \hat{r}p^- - s(u^-)v^- + \hat{s}v^-$$

and the extra term Θ is given by

$$\Theta = [F(u)] - \hat{f}[u] - [G(q)] + \hat{g}[q] + [H(l)] - \hat{h}[l] + [r(u)p] - \hat{r}[p] - \hat{r'}\hat{p}[u]$$
$$+[s(u)v] - \hat{s}[v] - \hat{s'}\hat{v}[u] - [wz] + \hat{z}[w] + \hat{w}[z].$$

Here

$$F(u) = \int^u f(u)du, \qquad G(q) = \int^q g(q)dq, \qquad H(l) = \int^l h(l)dl$$

and $[v] = v^+ - v^-$ denotes the jump of v.

With the definition (2.12) of the numerical fluxes and with simple algebraic manipulations, we easily obtain

$$[r(u)p] - \hat{r}[p] - \hat{r'}\hat{p}[u] = 0, \qquad [s(u)v] - \hat{s}[v] - \hat{s'}\hat{v}[u] = 0, \qquad -[wz] + \hat{z}[w] + \hat{w}[z] = 0$$

and hence

$$\Theta = [F(u)] - \hat{f}[u] - [G(q)] + \hat{g}[q] + [H(l)] - \hat{h}[l]$$
$$= \int_{u^-}^{u^+} (f(\tau) - \hat{f}(u^-, u^+))d\tau - \int_{q^-}^{q^+} (g(\tau) - \hat{g}(q^-, q^+))d\tau + \int_{l^-}^{l^+} (h(\tau) - \hat{h}(l^-, l^+))d\tau \ge 0$$

where the last inequality follows from the monotonicity of the fluxes $\hat{f}$, $-\hat{g}$ and $\hat{h}$. Hence

$$\int_{I_j} u_t u dx + \hat{\Phi}_{j+\frac{1}{2}} - \hat{\Phi}_{j-\frac{1}{2}} \le 0$$

which is the cell entropy inequality. Summing over all j and taking into account the periodic boundary condition, we obtain

$$\int_I u_t u dx \le 0.$$

This is the L^2 stability.

2.3. L^{n+1} stable schemes for the $K(n,n,n)$ equations

In this section, following the technique introduced in [24], we present and analyze a local discontinuous Galerkin method for which we can prove L^{n+1} stability for odd n. Consider the $K(n,n,n)$ equation

$$u_t + \alpha(u^n)_x + \beta(u^n)_{xxx} + \gamma(u^n)_{xxxxx} = 0 \tag{2.13}$$

with initial data

$$u(x,0) = u_0(x)$$

and periodic boundary conditions. Here α, β and γ are constants.

To define a local discontinuous Galerkin method, we rewrite the equation (2.13) as a first order system:

$$\begin{aligned} &u_t + \alpha v_x + p_x + w_x = 0, \qquad p - \beta q_x = 0, \quad q - v_x = 0, \quad w - h_x = 0, \\ &h - \gamma s_x = 0, \quad s - z_x = 0, \quad z - v_x = 0, \qquad v - u^n = 0. \end{aligned} \tag{2.14}$$

We can use the discontinuous Galerkin method to solve (2.14), resulting in the following scheme: find $u, p, q, w, h, s, z, v \in V_{\Delta x}$ such that, for all test functions $\rho, \phi, \varphi, \psi, \eta, \xi, \zeta, g \in V_{\Delta x}$,

$$\begin{aligned} &\int_{I_j} u_t \rho dx - \int_{I_j} (\alpha v + p + w)\rho_x dx + (\alpha\tilde{v} + \hat{p} + \hat{w})_{j+\frac{1}{2}} \rho^-_{j+\frac{1}{2}} - (\alpha\tilde{v} + \hat{p} + \hat{w})_{j-\frac{1}{2}} \rho^+_{j-\frac{1}{2}} = 0 \\ &\int_{I_j} p\phi dx + \beta \int_{I_j} q\phi_x dx - \beta \hat{q}_{j+\frac{1}{2}} \phi^-_{j+\frac{1}{2}} + \beta \hat{q}_{j-\frac{1}{2}} \phi^+_{j-\frac{1}{2}} = 0 \\ &\int_{I_j} q\varphi dx + \int_{I_j} v\varphi_x dx - \bar{v}_{j+\frac{1}{2}} \varphi^-_{j+\frac{1}{2}} + \bar{v}_{j-\frac{1}{2}} \varphi^+_{j-\frac{1}{2}} = 0 \\ &\int_{I_j} w\psi dx + \int_{I_j} h\psi_x dx - \hat{h}_{j+\frac{1}{2}} \psi^-_{j+\frac{1}{2}} + \hat{h}_{j-\frac{1}{2}} \psi^+_{j-\frac{1}{2}} = 0 \\ &\int_{I_j} h\eta dx + \gamma \int_{I_j} s\eta_x dx - \gamma \hat{s}_{j+\frac{1}{2}} \eta^-_{j+\frac{1}{2}} + \gamma \hat{s}_{j-\frac{1}{2}} \eta^+_{j-\frac{1}{2}} = 0 \\ &\int_{I_j} s\xi dx + \int_{I_j} z\xi_x dx - \hat{z}_{j+\frac{1}{2}} \xi^-_{j+\frac{1}{2}} + \hat{z}_{j-\frac{1}{2}} \xi^+_{j-\frac{1}{2}} = 0 \\ &\int_{I_j} z\zeta dx + \int_{I_j} v\zeta_x dx - \hat{v}_{j+\frac{1}{2}} \zeta^-_{j+\frac{1}{2}} + \hat{v}_{j-\frac{1}{2}} \zeta^+_{j-\frac{1}{2}} = 0 \\ &\int_{I_j} vg dx - \int_{I_j} u^n g dx = 0. \end{aligned} \tag{2.15}$$

The "hat" terms in (2.15) are the numerical fluxes. It turns out that we can again take the simple choices such that if $\alpha, \beta, \gamma > 0$,

$$\tilde{v} = v^-,\ \hat{p} = p^+,\ \hat{q} = q^+,\ \bar{v} = v^-,\ \hat{w} = w^+,\ \ \hat{h} = h^-,\ \hat{s} = s^-,\ \hat{z} = z^+,\ \hat{v} = v^-, \tag{2.16}$$

and if $\alpha, \beta, \gamma < 0$,

$$\tilde{v} = v^+,\ \hat{p} = p^+,\ \hat{q} = q^-,\ \bar{v} = v^-,\ \hat{w} = w^+,\ \ \hat{h} = h^-,\ \hat{s} = s^+,\ \hat{z} = z^+,\ \hat{v} = v^-. \tag{2.17}$$

Fluxes for other combinations of signs for α, β and γ can be obtained similarly.

We remark that the choice for the fluxes (2.16) and (2.17) are not unique. In fact the crucial part is taking $\hat{p}$ and $\bar{v}$ from opposite sides, $\hat{h}$ and $\hat{z}$ from opposite sides, and $\hat{w}$ and $\hat{v}$ from opposite sides.

With such a choice of fluxes we have

Proposition 2.5 (L^{n+1} stability). *The solution to the scheme (2.15) - (2.16) or (2.15) - (2.17) satisfies the L^{n+1} stability*

$$\frac{d}{dt}\int_0^L u^{n+1}(x,t)dx \le 0$$

for odd n.

Proof. We assume $\alpha,\beta,\gamma>0$ and take the fluxes as (2.16). Since (2.15) holds for any test functions in $V_{\Delta x}$, we can choose

$$\rho = v,\ \ \phi = q,\ \ \varphi = -p,\ \ \psi = z,\ \ \eta = -s,\ \ \xi = h,\ \ \zeta = -w,\ \ g = u_t.$$

Summing up the first seven equations in (2.15) we can get

$$\begin{aligned}
&\int_{I_j} u_t v dx - \alpha\int_{I_j} v v_x dx + \alpha\tilde{v}_{j+\frac{1}{2}}v^-_{j+\frac{1}{2}} - \alpha\tilde{v}_{j-\frac{1}{2}}v^+_{j-\frac{1}{2}}\\
+\beta&\int_{I_j} q q_x dx - \beta\hat{q}_{j+\frac{1}{2}}q^-_{j+\frac{1}{2}} + \beta\hat{q}_{j-\frac{1}{2}}q^+_{j-\frac{1}{2}} + \gamma\int_{I_j} s s_x dx - \gamma\hat{s}_{j+\frac{1}{2}}s^-_{j+\frac{1}{2}} + \gamma\hat{s}_{j-\frac{1}{2}}s^+_{j-\frac{1}{2}}\\
&-\int_{I_j}(pv)_x dx + \hat{p}_{j+\frac{1}{2}}v^-_{j+\frac{1}{2}} - \hat{p}_{j-\frac{1}{2}}v^+_{j-\frac{1}{2}} + \bar{v}_{j+\frac{1}{2}}p^-_{j+\frac{1}{2}} - \bar{v}_{j-\frac{1}{2}}p^+_{j-\frac{1}{2}}\\
&-\int_{I_j}(wv)_x dx + \hat{w}_{j+\frac{1}{2}}w^-_{j+\frac{1}{2}} - \hat{w}_{j-\frac{1}{2}}w^+_{j-\frac{1}{2}} + \hat{v}_{j+\frac{1}{2}}w^-_{j+\frac{1}{2}} - \hat{v}_{j-\frac{1}{2}}w^+_{j-\frac{1}{2}}\\
&+\int_{I_j}(hz)_x dx - \hat{h}_{j+\frac{1}{2}}z^-_{j+\frac{1}{2}} + \hat{h}_{j-\frac{1}{2}}z^+_{j-\frac{1}{2}} - \hat{z}_{j+\frac{1}{2}}h^-_{j+\frac{1}{2}} + \hat{z}_{j-\frac{1}{2}}h^+_{j-\frac{1}{2}} = 0.
\end{aligned}$$

With the definition (2.16) of the numerical fluxes, denoting

$$\Theta = \frac{1}{2}(v^+ - v^-)^2 + \frac{1}{2}(q^+ - q^-)^2 + \frac{1}{2}(s^+ - s^-)^2 \ge 0,$$

summing over j and taking into account the periodic boundary condition, we obtain

$$\int_0^L u_t v dx + \sum_j \Theta_{j-\frac{1}{2}} = 0,$$

hence $\int_0^L u_t v dx \le 0$, and with the last equation of (2.15) we have

$$\frac{d}{dt}\int_0^L u^{n+1}dx \le 0.$$

This is the L^{n+1} stability for odd n.

3. Numerical Results

In this section we provide numerical examples to illustrate the accuracy and capability of the method for these nonlinear wave equations. Time discretization is either by the third order explicit Runge-Kutta method in [27] or by the third-order semi-implicit Runge-Kutta method in [32]. In all examples, the figures present the solution obtained with a particular choice of the mesh. We have verified with the aid of successive mesh refinements, that in all cases, the results shown are numerically convergent.

3.1. The KdVB equation

First, we approximate solutions of the KdVB equation

$$u_t + \varepsilon u u_x - \alpha u_{xx} + \beta u_{xxx} = 0. \tag{3.1}$$

Table 3.1: Accuracy test for the KdVB equation (3.1) with the exact solution (3.2). $\varepsilon = \alpha = \beta = 1$, $x_0 = 0$. Exact boundary condition. Uniform and non-uniform meshes with N cells at time $t = 1$.

		uniform mesh				non-uniform mesh			
	N	L^2 error	order	L^∞ error	order	L^2 error	order	L^∞ error	order
p^0	40	1.02E-02	–	6.90E-02	–	1.03E-02	–	7.49E-02	–
	80	5.14E-03	0.99	3.54E-02	0.96	5.20E-03	0.99	3.82E-02	0.97
	160	2.57E-03	1.00	1.77E-02	1.00	2.62E-03	0.99	2.10E-02	0.86
	320	1.23E-03	1.00	8.91E-03	1.00	1.31E-03	1.00	1.05E-02	1.00
p^1	40	1.35E-03	–	1.40E-02	–	1.30E-03	–	1.28E-02	–
	80	3.51E-04	1.94	3.76E-03	1.90	3.61E-04	1.86	3.97E-03	1.69
	160	8.87E-05	1.99	9.52E-04	1.98	9.13E-05	1.98	1.12E-03	1.83
	320	2.23E-05	1.99	2.38E-04	2.00	2.29E-05	1.99	2.80E-04	2.00
p^2	40	1.15E-04	–	1.87E-03	–	1.55E-04	–	2.63E-03	–
	80	1.24E-05	3.21	1.95E-04	3.26	1.36E-05	3.51	2.26E-04	3.54
	160	1.56E-06	2.99	2.51E-05	2.95	1.67E-06	3.02	3.33E-05	2.76
	320	1.95E-07	3.00	3.14E-06	3.00	2.09E-07	3.00	4.18E-06	2.99
p^3	40	1.38E-05	–	1.36E-04	–	1.05E-05	–	9.73E-05	–
	80	9.30E-07	3.89	1.27E-05	3.42	1.02E-06	3.36	1.30E-05	2.90
	160	5.97E-08	3.96	8.54E-07	3.89	6.62E-08	3.94	1.06E-06	3.62
	320	3.76E-09	3.99	5.38E-08	3.99	4.17E-09	3.99	7.32E-08	3.86

Example 3.1. We show an accuracy test for the equation (3.1) with the exact solution

$$u(x,t) = -\frac{3\alpha^2}{25\varepsilon\beta}\left(-\mathrm{sech}^2(k(x-x_0)-ct) + 2\tanh(k(x-x_0)-ct)+2\right) \tag{3.2}$$

where $k = \dfrac{\alpha}{10\beta}$ and $c = \dfrac{3\alpha^3}{125\beta^2}$. Both uniform and nonuniform meshes are used. The non-uniform meshes in this and later examples are a repeated pattern of $0.9\Delta x$ and $1.1\Delta x$ with an even number of elements. The L^2 and L^∞ errors and the numerical order of accuracy are contained in Table 3.1 for the uniform and nonuniform mesh cases. We can see that the method with P^k elements gives a uniform $(k+1)$-th order of accuracy in both norms for both the uniform and non-uniform meshes.

Example 3.2. In this example we show KdV type solutions for the equation (3.1) to see the birth of solitons from the Gaussian initial condition

$$u(x,0) = e^{-x^2} \tag{3.3}$$

with boundary conditions

$$u(-15,t) = u(15,t) = 0, \quad t > 0 \tag{3.4}$$

In Figure 3.1 we can clearly see that the initial Gaussian breaks up into a number of solitons. Comparing with the results obtained by the quintic B-spline finite element scheme in [33], we can see that our methods use fewer cells (about half) to get the same result.

Example 3.3. We compute the KdVB type solutions for the equation (3.1) with the initial condition

$$u(x,0) = 0.5\left(1 - \tanh\frac{|x|-x_0}{d}\right) \tag{3.5}$$

to see the effect of using different values of α and β.

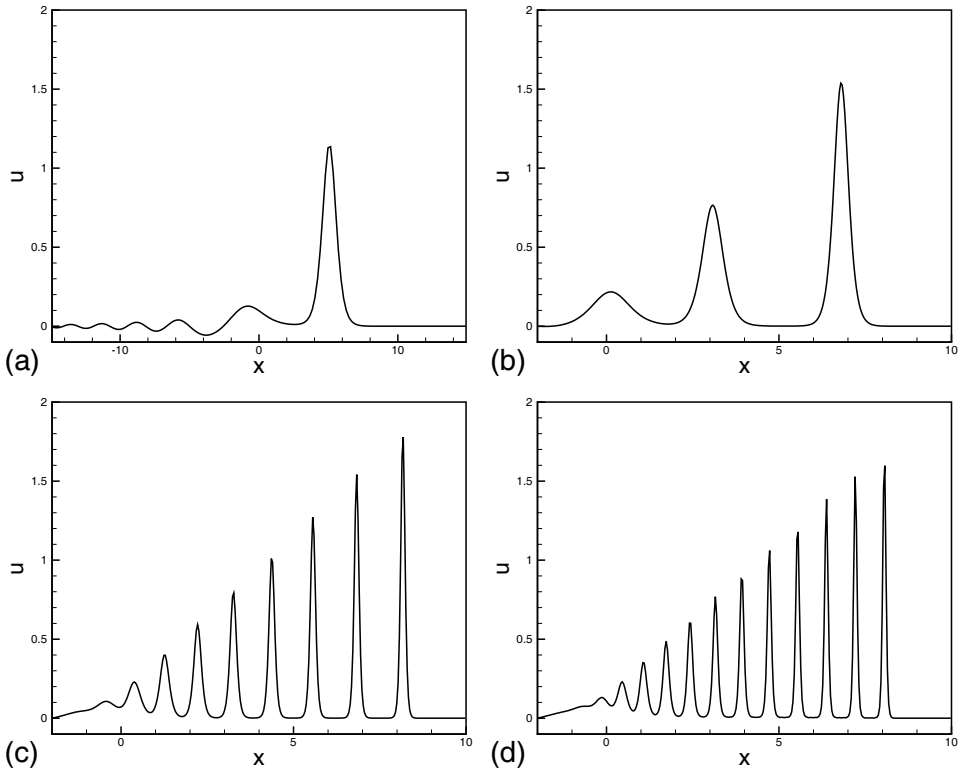

Figure 3.1: KdV type solutions with the Gaussian initial condition (3.3) at time $t = 12.5$, $\alpha = 0$ and $\varepsilon = 1$. (a) $\beta = 0.04$, one soliton plus an oscillating tail, P^1 elements with 160 cells; (b) $\beta = 0.01$, three solitons, P^1 elements with 320 cells; (c) $\beta = 0.001$, nine solitons, P^2 elements with 320 cells; (d) $\beta = 0.0005$, twelve solitons, P^2 elements with 320 cells.

In Figure 3.2 we take the boundary conditions

$$u(-50, t) = u(150, t) = 0. \tag{3.6}$$

We can see that the solution of the KdVB equation (3.1) tends to behave like a solution of the viscous Burgers equation as we increase α.

Next, in Figure 3.3 we proceed to take the boundary conditions

$$u(0, t) = 1, \qquad u(150, t) = 0. \tag{3.7}$$

As α is decreased, the computed solutions of the KdVB equation (3.1) become more oscillatory.

3.2. The fifth-order KdV equations

In the following examples we present results for the fifth-order KdV type equations with linear higher derivative terms.

Example 3.4. We show an accuracy test for the Kawahara equation

$$u_t + uu_x + u_{xxx} - u_{xxxxx} = 0 \tag{3.8}$$

with the exact solution [29]

$$u(x, t) = \frac{105}{169}\text{sech}^4\left(\frac{1}{2\sqrt{13}}(x - \frac{36}{169}t - x_0)\right). \tag{3.9}$$

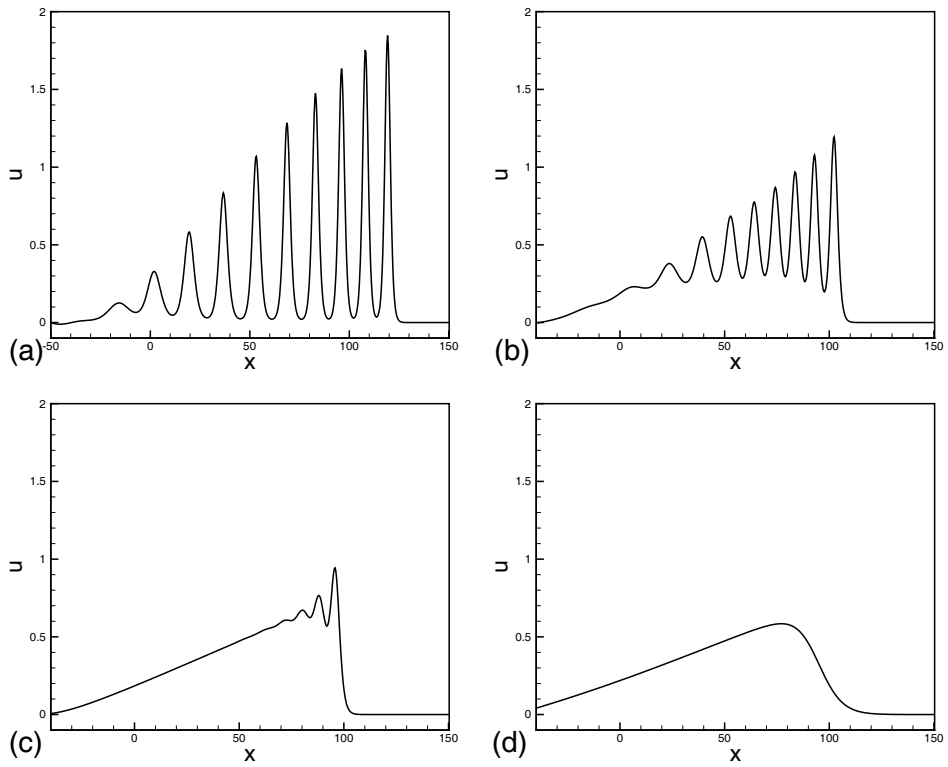

Figure 3.2: KdVB type solutions with the initial condition (3.5) and the boundary conditions (3.6) at time $t = 800$, $-50 \le x \le 150$, $d = 5$, $x_0 = 25$, $\varepsilon = 0.2$ and $\beta = 0.1$. (a) $\alpha = 0.0001$, P^1 elements with 640 cells; (b) $\alpha = 0.005$, P^1 elements with 640 cells; (c) $\alpha = 0.03$, P^1 elements with 640 cells; (d) $\alpha = 0.4$, P^1 elements with 320 cells.

Table 3.2: Accuracy test for the Kawahara equation (3.8) with the exact solution (3.9). Periodic boundary condition, $x_0 = 0$. Uniform and non-uniform meshes with N cells at $t = 1$.

		uniform mesh				non-uniform mesh			
	N	L^2 error	order	L^∞ error	order	L^2 error	order	L^∞ error	order
p^0	20	3.20E-02	–	1.20E-01	–	3.24E-02	–	1.36E-01	–
	40	1.68E-02	0.93	6.33E-02	0.91	1.71E-02	0.93	7.30E-02	0.89
	80	8.61E-03	0.97	3.38E-02	0.91	8.76E-03	0.96	3.86E-02	0.92
	160	4.36E-03	0.98	1.73E-02	0.97	4.44E-03	0.98	1.99E-02	0.95
p^1	20	6.47E-03	–	5.31E-02	–	6.59E-03	–	5.97E-02	–
	40	1.68E-03	1.94	1.48E-02	1.84	1.73E-03	1.93	1.73E-02	1.79
	80	4.27E-04	1.98	3.81E-03	1.96	4.39E-04	1.98	4.47E-03	1.95
	160	1.07E-04	1.99	9.58E-04	1.99	1.11E-04	1.99	1.13E-03	1.99
p^2	20	5.46E-04	–	3.91E-03	–	6.13E-04	–	4.67E-03	–
	40	6.77E-05	3.01	5.80E-04	2.75	7.35E-05	3.06	7.37E-04	2.66
	80	8.49E-06	3.00	7.53E-05	2.95	9.10E-06	3.01	9.99E-05	2.88
	160	1.39E-06	2.62	9.76E-06	2.95	1.45E-06	2.65	1.27E-05	2.97

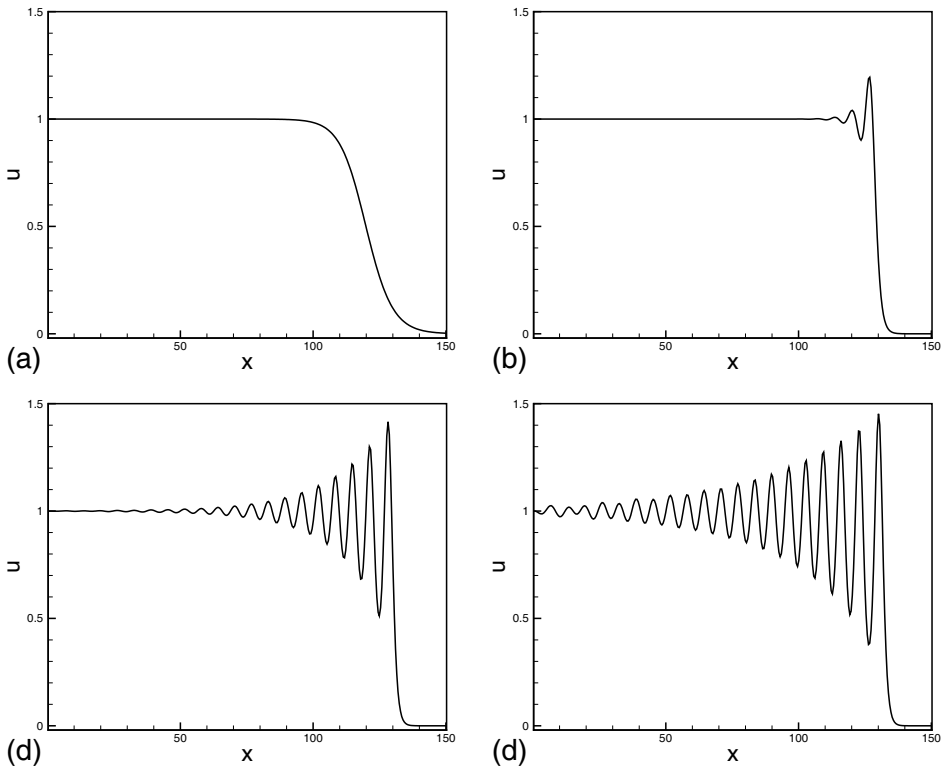

Figure 3.3: KdVB type solutions with the initial condition (3.5) and the boundary conditions (3.7) at time $t = 800$, $0 \le x \le 150$, $d = 5$, $x_0 = 50$, $\varepsilon = 0.2$ and $\beta = 0.1$. (a) $\alpha = 0.5$, P^1 elements with 320 cells; (b) $\alpha = 0.05$, P^1 elements with 320 cells; (c) $\alpha = 0.01$, P^1 elements with 320 cells; (d) $\alpha = 0.005$, P^1 elements with 320 cells.

We can see in Table 3.2 that the method with P^k elements gives $(k+1)$-th order of accuracy in both L^2 and L^∞ norms for both the uniform and non-uniform meshes.

Example 3.5. We show an accuracy test for generalized Kawahara equation

$$u_t + \sigma u u_x + u^2 u_x + u_{xxx} - u_{xxxxx} = 0 \tag{3.10}$$

with the exact solution

$$u(x,t) = -6\sqrt{10}k^2 \operatorname{sech}^2\left(k(x - c\,t - x_0)\right) \tag{3.11}$$

where $c = 4k^2(1-4k^2)$, $k^2 = \dfrac{1}{20} + \dfrac{\sigma}{4\sqrt{10}}$ and $\sigma = \dfrac{2}{\sqrt{90}}$. We can see in Table 3.3 that the method with P^k elements gives $(k+1)$-th order of accuracy in both L^2 and L^∞ norms for both the uniform and non-uniform meshes.

Example 3.6. Ito's fifth-order mKdV equation [22]

$$u_t + \left(6u^5 + 5\alpha u (u^2)_{xx} - u_{xxxx}\right)_x = 0. \tag{3.12}$$

When $\alpha = -1$, an exact solution is

$$u(x,t) = k \tanh\left(k(x - c\,t - x_0)\right) \tag{3.13}$$

Table 3.3: Accuracy test for the generalized Kawahara equation (3.10) with the exact solution (3.11). Periodic boundary condition, $x_0 = 0$. Uniform and non-uniform meshes with N cells at time $t = 1$.

		uniform mesh				non-uniform mesh			
	N	L^2 error	order	L^∞ error	order	L^2 error	order	L^∞ error	order
p^0	20	7.71E-02	–	2.73E-01	–	7.86E-02	–	3.01E-01	–
	40	4.59E-02	0.75	1.80E-01	0.60	4.65E-02	0.76	1.84E-01	0.71
	80	2.58E-02	0.83	1.10E-01	0.71	2.62E-02	0.83	1.12E-01	0.71
	160	1.39E-02	0.90	6.05E-02	0.86	1.41E-02	0.90	6.09E-02	0.88
p^1	20	1.74E-02	–	1.48E-01	–	1.76E-02	–	1.62E-01	–
	40	4.69E-03	1.89	4.73E-02	1.65	4.81E-03	1.87	5.47E-02	1.57
	80	1.21E-03	1.95	1.28E-02	1.89	1.25E-03	1.95	1.50E-02	1.86
	160	3.09E-04	1.97	3.27E-03	1.97	3.18E-04	1.97	3.85E-03	1.96
p^2	20	2.42E-03	–	1.73E-02	–	2.63E-03	–	2.10E-02	–
	40	2.68E-04	3.17	2.84E-03	2.61	2.92E-04	3.17	3.19E-03	2.71
	80	3.36E-05	3.00	3.49E-04	3.03	3.61E-05	3.02	4.63E-04	2.79
	160	4.35E-06	2.95	4.4E-05	2.97	4.65E-06	2.95	5.90E-05	2.97

Table 3.4: Accuracy test for the Ito's fifth-order mKdV equation (3.12) with the exact solution (3.13), $k = 0.1$, $x_0 = 0$. Exact boundary condition. Uniform and non-uniform meshes with N cells at time $t = 1$.

		uniform mesh				non-uniform mesh			
	N	L^2 error	order	L^∞ error	order	L^2 error	order	L^∞ error	order
p^0	20	5.52E-03	–	2.45E-02	–	5.55E-03	–	2.68E-02	–
	40	2.76E-03	1.00	1.24E-02	0.98	2.78E-03	1.00	1.40E-02	0.94
	80	1.38E-03	1.00	6.24E-03	0.99	1.41E-03	0.98	7.42E-03	0.91
	160	6.91E-04	1.00	3.13E-03	1.00	7.04E-04	1.00	3.71E-03	1.00
p^1	20	6.25E-04	–	3.78E-03	–	6.54E-04	–	3.88E-03	–
	40	1.62E-04	1.95	1.00E-03	1.92	1.67E-04	1.97	1.08E-03	1.85
	80	4.06E-05	2.01	2.51E-04	2.00	4.18E-05	2.00	2.92E-04	1.88
	160	1.01E-05	2.00	6.28E-05	2.00	1.04E-05	2.00	7.38E-05	1.99
p^2	20	3.68E-005	–	3.55E-004	–	4.41E-005	–	4.27E-004	–
	40	4.82E-006	2.93	5.02E-005	2.82	5.48E-006	3.01	6.78E-005	2.65
	80	5.98E-007	3.01	6.46E-006	2.96	6.41E-007	3.10	8.51E-006	2.99
	160	8.22E-008	2.86	8.10E-007	2.99	8.71E-008	2.88	1.08E-006	2.98

where $c = 6k^4$, k is an arbitrary constant. We can see in Table 3.4 that the method with P^k elements gives $(k+1)$-th order of accuracy in both L^2 and L^∞ norms for both the uniform and non-uniform meshes.

We also present the shock profile wave propagation for Ito's fifth-order mKdV equation (3.12) in Figure 3.4 with the initial condition

$$u(x, 0) = k \tanh(k(x - x_0)) \tag{3.14}$$

for different k.

Example 3.7. Solitons of the fifth-order KdV type equations with high nonlinearities [17]

$$u_t + u^p u_x + u_{xxx} - \delta u_{xxxxx} = 0. \tag{3.15}$$

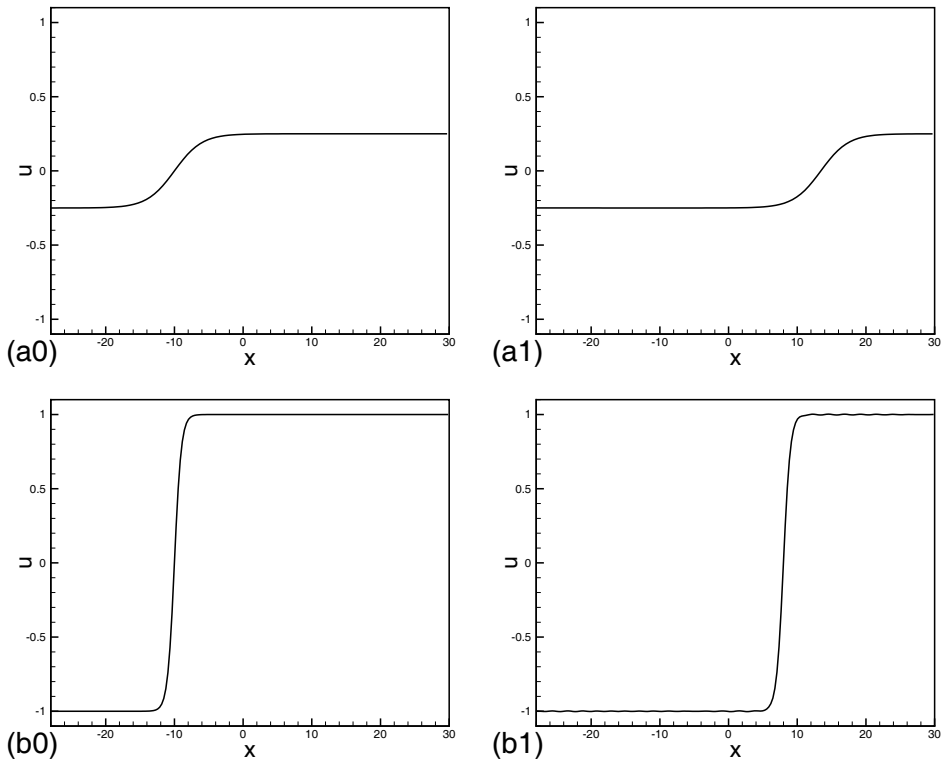

Figure 3.4: The shock profile wave propagation of the Ito's fifth-order mKdV equation (3.12) with initial condition (3.14). Exact boundary condition for different k. (a0) $k = 0.25$, $t = 0$; (a1) $k = 0.25$, $t = 1000$, P^1 elements with 100 cells; (b0) $k = 1$, $t = 0$; (b1) $k = 1$, $t = 3$, P^1 elements with 200 cells;

Solitary wave solutions of equation (3.15) are unstable with respect to the collapse-type instabilities if $p \geq 4$ for $\delta = 0$. When $\delta \neq 0$, i.e., with the addition of the fifth-order term, solitons become stable also for certain $p \geq 4$. The exact upper limit of the nonlinearity parameter p for stability is still an open problem. We present the numerical results of the equation (3.15) in Figure 3.5 for $p = 4$ and different $\delta > 0$ with the initial condition

$$u(x,0) = \left(\frac{k}{8}\frac{(p+1)(p+4)(3p+4)}{p+2}\right)^{\frac{1}{p}} \operatorname{sech}^{\frac{4}{p}}\left(\frac{p\sqrt{k(p^2+4p+8)}}{4(p+2)}(x-x_0)\right) \tag{3.16}$$

where $k = \left(\dfrac{2(p+2)}{p^2+4p+8}\right)^2 \dfrac{1}{\delta}$.

Next we present numerical results of the equation (3.15) in Figure 3.6 for $p = 2$ and different $\delta < 0$ with initial condition

$$u(x,0) = 3\sqrt{\frac{2}{5\delta}}\operatorname{sech}\left(\sqrt{\frac{1}{10\delta}}x\right)\tanh\left(\sqrt{\frac{1}{10\delta}}(x-x_0)\right). \tag{3.17}$$

We have also made numerical experiments for $p = 1, 2, 3$ and different $\delta > 0$ with the initial condition (3.16), but we will not show the results to save space.

Example 3.8. In this example we show the soliton interaction for the Kawahara equation

$$u_t + uu_x + u_{xxx} - \delta u_{xxxxx} = 0. \tag{3.18}$$

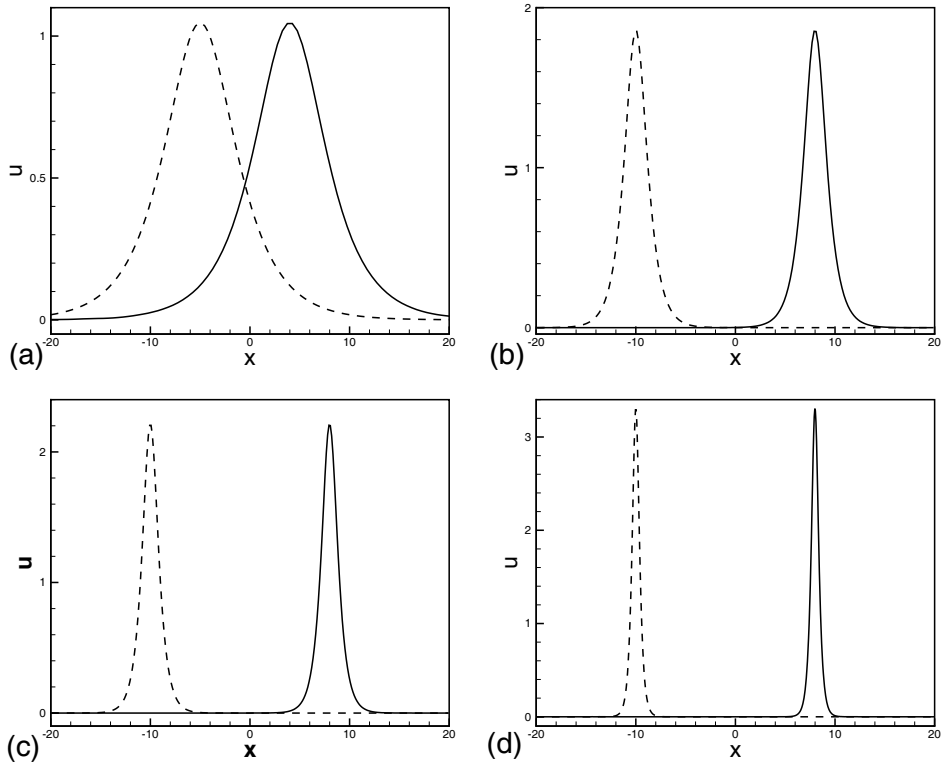

Figure 3.5: Solitons of the fifth-order KdV type equation (3.15) with initial condition (3.16), p=4. Periodic boundary condition for different δ. Dashed line is at $t = 0$. (a) $\delta = 1$, $t = 100$, P^2 elements with 100 cells; (b) $\delta = 0.1$, $t = 20$, P^2 elements with 200 cells; (c) $\delta = 0.05$, $t = 10$, P^2 elements with 300 cells; (d) $\delta = 0.01$, $t = 2$, P^2 elements with 700 cells.

The double soliton collision case has the initial condition

$$u(x,0) = \frac{105}{338\delta_1}\operatorname{sech}^4\left(\frac{1}{2\sqrt{13\delta_1}}(x-x_1)\right) + \frac{105}{338\delta_2}\operatorname{sech}^4\left(\frac{1}{2\sqrt{13\delta_2}}(x-x_2)\right) \tag{3.19}$$

where $\delta = 0.1$, $\delta_1 = 0.04 \times 338/105$, $\delta_2 = 0.15 \times 338/105$, $x_1 = -10$ and $x_2 = -4$. The solution is computed with periodic boundary condition in [-18,18] using P^2 elements with 200 cells and is shown in Figure 3.7.

The triple soliton splitting case has the initial condition

$$u(x,0) = \frac{1}{\delta_1}\operatorname{sech}^4\left(\frac{1}{2\sqrt{13\delta_1}}(x-x_1)\right) + \frac{1}{\delta_2}\operatorname{sech}^4\left(\frac{1}{2\sqrt{13\delta_2}}(x-x_2)\right) + \frac{1}{\delta_3}\operatorname{sech}^4\left(\frac{1}{2\sqrt{13\delta_3}}(x-x_3)\right) \tag{3.20}$$

where $\delta = 0.1$, $\delta_1 = 0.25$, $\delta_2 = 0.35$, $\delta_3 = 0.45$, $x_1 = -11$, $x_2 = -9$ and $x_3 = -7$. The solution is computed with periodic boundary condition in [-20,20] using P^2 elements with 200 cells and is shown in Figure 3.8.

Next we proceed to take the compact initial condition

$$u_0(x) = \begin{cases} A\cos^2(Bx - C) & |Bx - C| \le \pi/2 \\ 0 & \text{otherwise} \end{cases} \tag{3.21}$$

In Figure 3.9 we can see the pulsating multiplet solution which has been shown in [21].

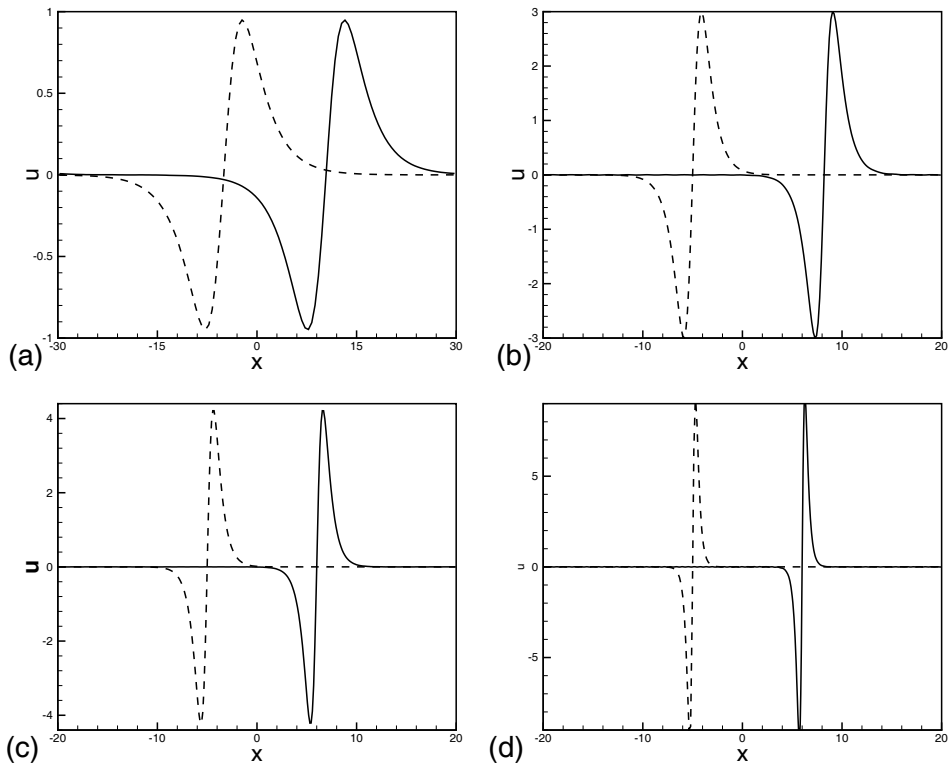

Figure 3.6: Solitons of the fifth-order KdV type equation (3.15) with initial condition (3.17), p=2. Periodic boundary condition using P^2 elements for different δ. Dashed line is at $t = 0$. (a) $\delta = -1$, $t = 140$, P^2 elements with 120 cells; (b) $\delta = -0.1$, $t = 12$, P^2 elements with 250 cells; (c) $\delta = -0.05$, $t = 5$, P^2 elements with 320 cells; (d) $\delta = -0.01$, $t = 1$, P^2 elements with 700 cells.

Example 3.9. In this example we present the more general type of "semi-localized" solitary wave solutions and their interactions [5] for the fifth-order KdV equation

$$u_t + uu_x + u_{xxx} + u_{xxxxx} = 0. \tag{3.22}$$

The tails of these oscillatory solitary wave solutions no longer decay to zero, but have finite amplitude oscillatory structures. These solutions are rigorously characterized in [20] as singular perturbations of the KdV solitons.

The examples about these "semi-localized" solitary wave solutions take the following initial condition

$$u(x, 0) = 12\varepsilon^2 \mathrm{sech}^2[\varepsilon(x - x_0)], \tag{3.23}$$

where ε is related to the size of the oscillations. Figure 3.10 shows the "semi-localized" solitary wave solutions and Figure 3.11 shows their interactions for different ε with the initial condition

$$u(x, 0) = 12\varepsilon^2 \left(\mathrm{sech}^2[\varepsilon(x - x_0)] + \mathrm{sech}^2[\varepsilon(x + x_0)]\right). \tag{3.24}$$

In Figure 3.12 we show the space time graph of the solutions up to $t = 20$ for the third and the fourth cases in Figure 3.11.

3.3. A generalized fifth-order KdV equation

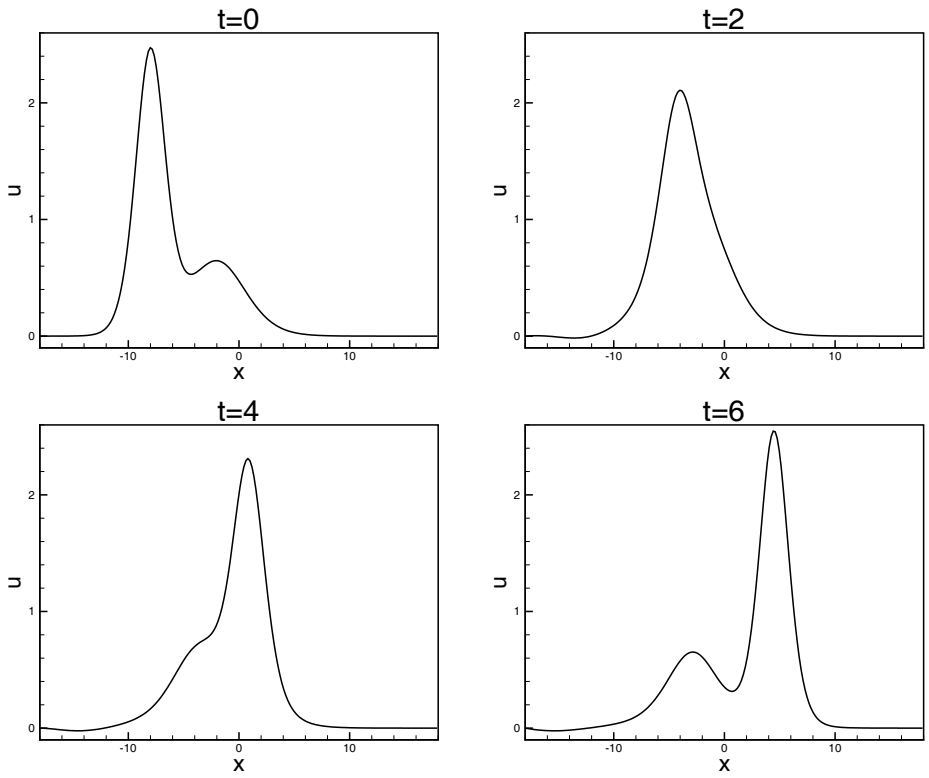

Figure 3.7: Double soliton collision profiles. Periodic boundary condition in [-18,18] using P^2 elements with 200 cells.

Example 3.10. In this example we first show the accuracy test result of a generalized fifth-order KdV equation [26]

$$u_t + (u^3)_x + (u(u^2)_{xx})_x + \delta(u(u^2)_{xxxx})_x = 0 \tag{3.25}$$

Notice that the highest order derivative term of equation (3.25) is also nonlinear. Equation (3.25) has compacton solutions of the form

$$u(x,t) = \begin{cases} \sqrt{\frac{8}{3}\lambda}\cos^2(\sqrt{\triangle_-}(x-\lambda t)/2) & |\sqrt{\triangle_-}(x-\lambda t)| \le \pi \\ 0 & \text{otherwise} \end{cases} \tag{3.26}$$

where $\triangle_- = (1-\sqrt{1-4\delta})/2\delta$. The degree of polynomials is taken as $k = 0, 1$. We can see in Table 3.5 that the method with P^k elements gives $(k+1)$-th order of accuracy in both L^2 and L^∞ norms for both the uniform and non-uniform meshes.

Next, we proceed to show the single compacton propagation in Figure 3.13 for the initial condition

$$u(x,0) = \begin{cases} \sqrt{\frac{8}{3}\lambda}\cos^2(\sqrt{\Delta_-}(x-x_0)/2) & |\sqrt{\Delta_-}(x-x_0)| \le \pi \\ 0 & \text{otherwise.} \end{cases} \tag{3.27}$$

We also show the single compacton propagation in Figure 3.14 for the initial condition

$$u(x,0) = \begin{cases} \sqrt{2\lambda[2-\cos(\sqrt{\Delta_-}(x-x_0))]}\cos^2(\sqrt{\Delta_-}(x-x_0)/2) & |\sqrt{\Delta_-}(x-x_0)| \le \pi \\ 0 & \text{otherwise.} \end{cases} \tag{3.28}$$

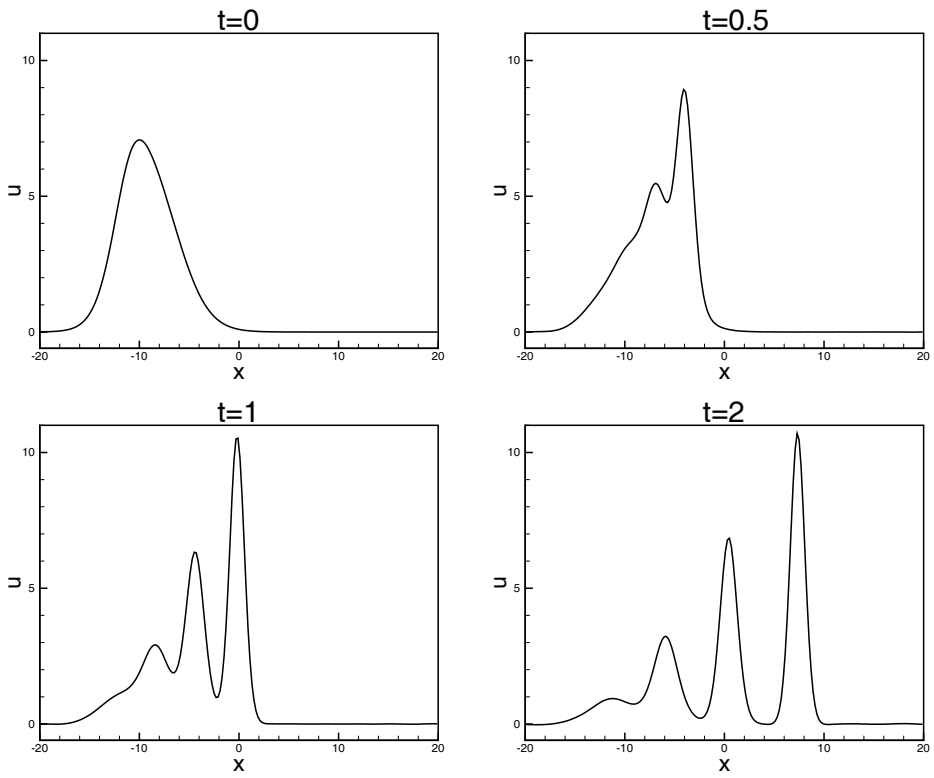

Figure 3.8: Triple soliton collision profiles. Periodic boundary condition in [-20,20] using P^2 elements with 200 cells.

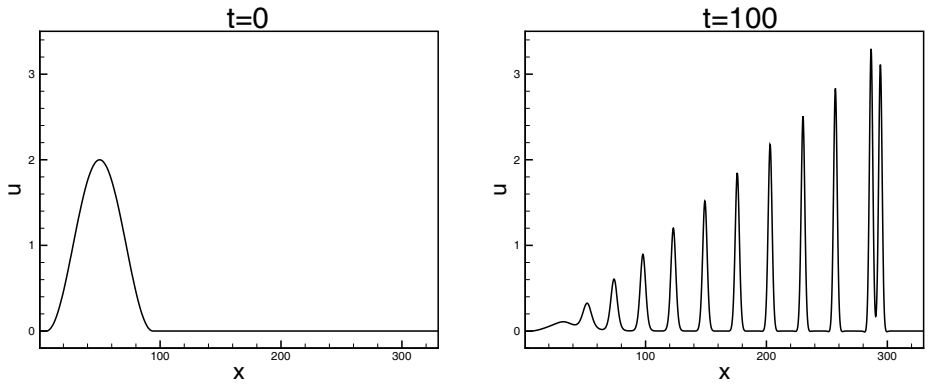

Figure 3.9: The pulsating multiplet solution with initial condition (3.21) for $\delta = 0.5$ in [0,330] using P^2 elements with 1500 cells, where $A = 2$, $B = 1/28$ and $C = 50/28$.

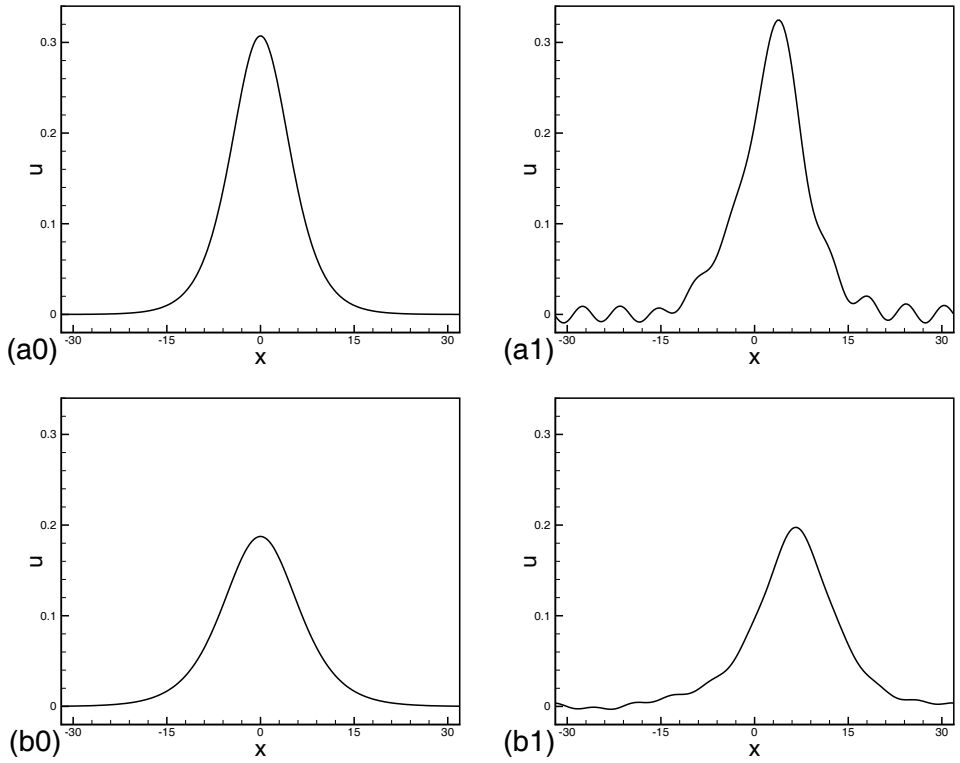

Figure 3.10: "Semi-localized" solitary wave solutions for the fifth-order KdV equation (3.22) with initial condition (3.23). Periodic boundary condition in [-32,32] using P^2 elements with 200 cells, $x_0 = 0$. (a0) $\varepsilon = 0.16$, $t = 0$; (a1) $\varepsilon = 0.16$, $t = 30$; (b0) $\varepsilon = 0.125$, $t = 0$; (b1) $\varepsilon = 0.125$, $t = 100$.

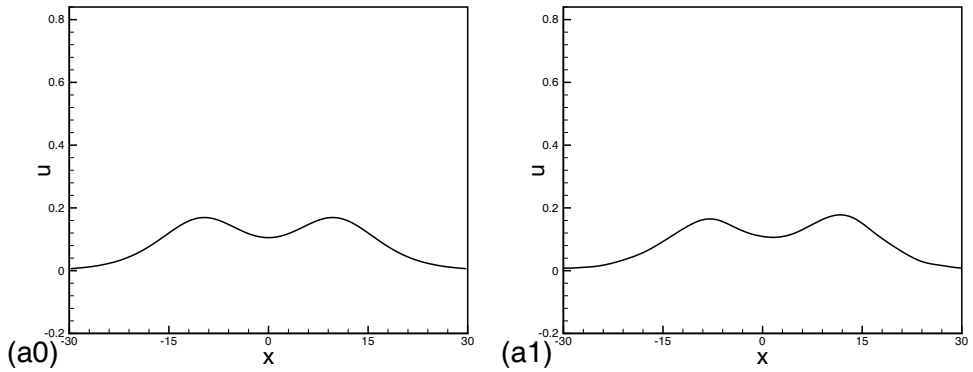

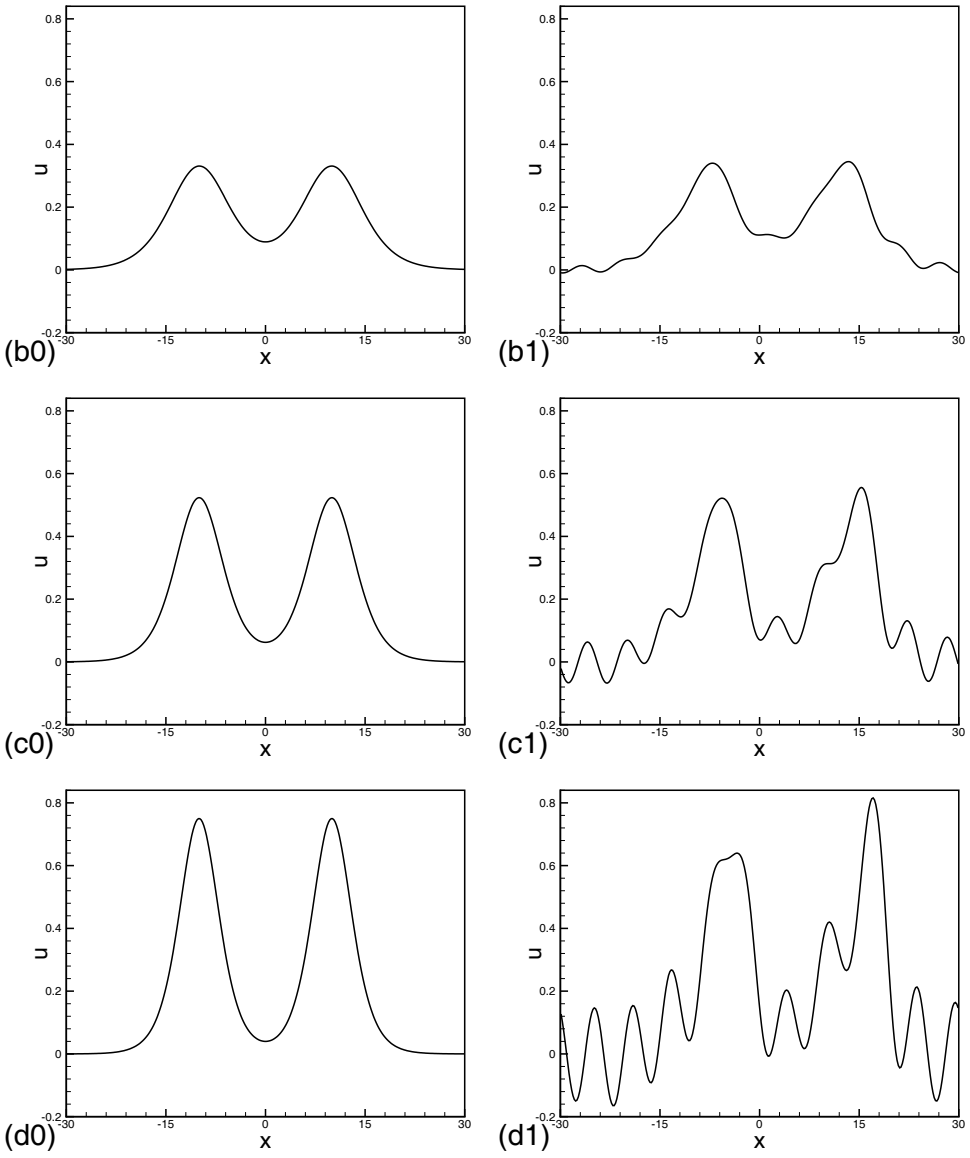

Figure 3.11: The interactions of the "semi-localized" solitary wave solutions for the fifth-order KdV equation (3.22) with initial condition (3.24). Periodic boundary condition in [-30,30] using P^2 elements with 300 cells at time t=20, $x_0 = 10$. (a0) $\varepsilon = 0.116573$, $t = 0$; (a1) $\varepsilon = 0.116573$, $t = 20$; (b0) $\varepsilon = 0.165639$, $t = 0$; (b1) $\varepsilon = 0.165639$, $t = 20$; (c0) $\varepsilon = 0.208756$, $t = 0$; (c1) $\varepsilon = 0.208756$, $t = 20$; (d0) $\varepsilon = 0.25$, $t = 0$; (d1) $\varepsilon = 0.25$, $t = 20$.

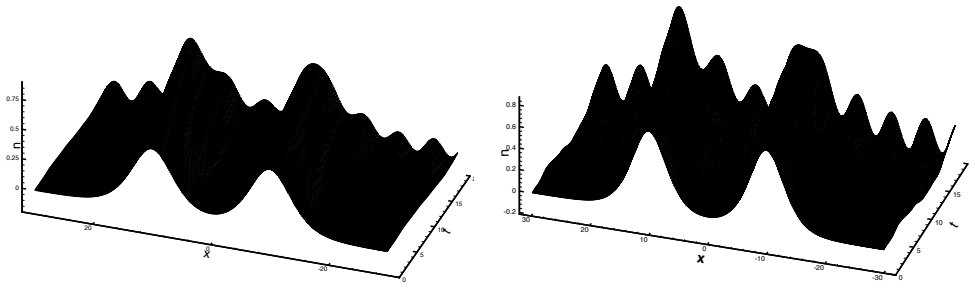

Figure 3.12: Space time graph of the "semi-localized" solitary wave solutions. The left is the third case in Figure 3.11 and the right is the fourth case in Figure 3.11.

Table 3.5: Accuracy test for the compacton solution (3.26) of the equation (3.25). $\delta = 0.16$. Uniform and non-uniform meshes with N cells at time $t = 1$.

		uniform mesh				non-uniform mesh			
	N	L^2 error	order	L^∞ error	order	L^2 error	order	L^∞ error	order
p^0	20	1.43E-02	–	8.53E-02	–	1.44E-02	–	8.94E-02	–
	40	7.17E-03	1.00	4.45E-02	0.94	7.23E-03	1.00	4.89E-02	0.87
	80	3.72E-03	0.95	2.49E-02	0.84	3.77E-03	0.94	2.50E-02	0.97
	160	1.90E-03	0.97	1.32E-02	0.91	1.94E-03	0.96	1.50E-02	0.74
p^1	20	5.73E-03	–	4.99E-02	–	5.97E-03	–	5.08E-02	–
	40	1.97E-03	1.54	1.89E-02	1.40	1.97E-03	1.60	2.02E-02	1.33
	80	5.02E-04	1.97	5.03E-03	1.91	5.10E-04	1.95	6.16E-03	1.72
	160	1.29E-04	1.96	1.30E-03	1.95	1.32E-04	1.95	1.54E-03	2.00

3.4. The fully nonlinear $K(n, n, n)$ equations

Example 3.11. In this example we first show the accuracy test result of the fully nonlinear $K(n, n, n)$ equations [16]

$$u_t + \alpha(u^n)_x + \beta(u^n)_{xxx} + \gamma(u^n)_{xxxxx} = 0 \tag{3.29}$$

The exact solution is

$$u(x,t) = \begin{cases} A_n \cos^\delta(B_n(x-\lambda t)) & |B_n(x-\lambda t)| \le \frac{\pi}{2} \\ 0 & \text{otherwise} \end{cases} \tag{3.30}$$

Where δ, A_n and B_n are constants for $n = 3, 5$ respectively. For the $K(3, 3, 3)$ equation,

$$\delta = 2, \;\; A_3 = 2\sqrt{\frac{2\lambda}{5\alpha}}, \;\; B_3 = \frac{1}{12}\sqrt{\frac{13\alpha}{\beta}}, \;\; \gamma = \frac{36\beta^2}{169\alpha}; \tag{3.31}$$

for the $K(5, 5, 5)$ equation,

$$\delta = 1, \;\; A_5 = \sqrt[4]{\frac{15\lambda}{8\alpha}}, \;\; B_5 = \frac{1}{15}\sqrt{\frac{34\alpha}{\beta}}, \;\; \gamma = \frac{225\beta^2}{1156\alpha}. \tag{3.32}$$

The accuracy is measured in smooth parts of the solution, $\pi/8$ away from the corners. We can see in Table 3.6 that the method with P^k elements gives $(k+1)$-th order of accuracy in both L^2 and L^∞ norms.

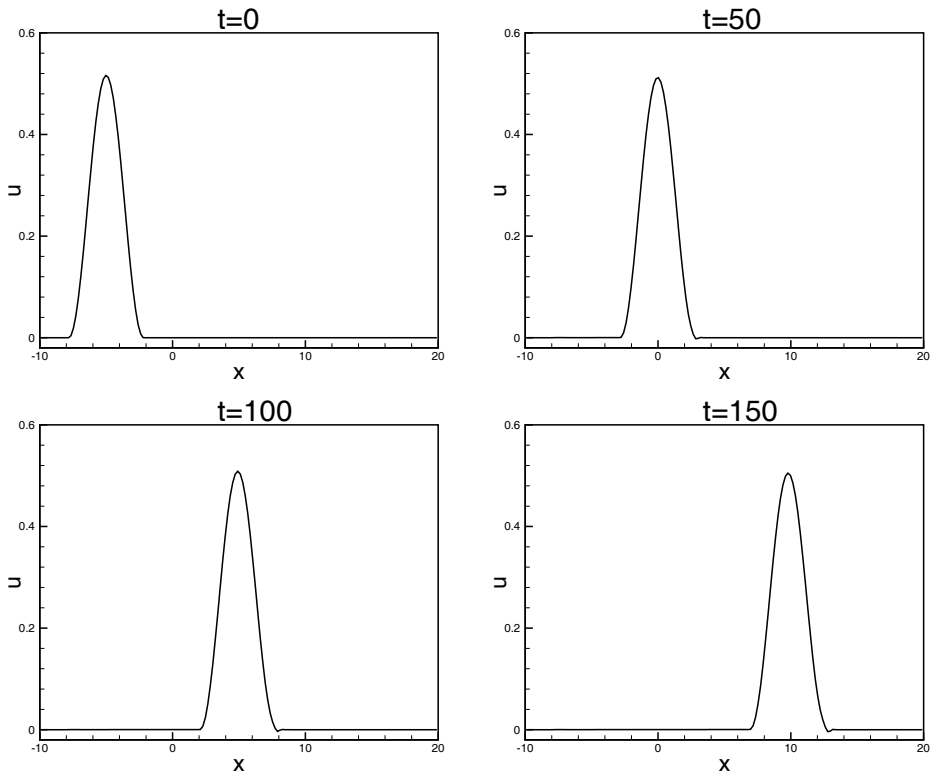

Figure 3.13: The single compacton. The initial data is taken as (3.27), where $\delta = 0.16$, $x_0 = -5$ and $\lambda = 0.1$. Using P^1 elements with 160 cells in [-10,20].

Table 3.6: Accuracy test for the compacton solution (3.30). The L^4 stable scheme for the $K(3,3,3)$ equation in [-20,20] and the L^6 stable scheme for the $K(5,5,5)$ equation in [-25,25]. L^2 and L^∞ errors. Nonuniform meshes with N cells in smooth parts of the solution with P^0, P^1, P^2 at time $T = 1.0$.

		$K(3,3,3)$				$K(5,5,5)$			
	n	L^2 error	order	L^∞ error	order	L^2 error	order	L^∞ error	order
p^0	20	2.45E-02	–	1.13E-01	–	2.35E-02	–	2.53E-01	–
	40	1.37E-02	0.84	7.79E-02	0.53	1.31E-02	0.84	1.07E-01	1.24
	80	7.74E-03	0.82	4.76E-02	0.71	7.59E-03	0.79	7.25E-02	0.56
	160	4.15E-03	0.90	2.54E-02	0.91	4.35E-03	0.80	3.93E-02	0.88
p^1	20	9.06E-03	–	7.93E-02	–	1.02E-02	–	8.96E-02	–
	40	3.22E-03	1.49	2.43E-02	1.70	4.02E-03	1.34	4.19E-02	1.10
	80	8.51E-04	1.92	9.14E-03	1.41	9.99E-04	2.01	1.19E-02	1.81
	160	2.23E-04	1.93	2.38E-03	1.94	2.41E-04	2.05	3.49E-03	1.77
p^2	20	2.55E-03	–	2.51E-02	–	3.244E-03	–	4.07E-02	–
	40	5.05E-04	2.34	9.18E-03	1.45	2.84E-04	3.51	2.72E-03	3.90
	80	6.06E-05	3.06	1.17E-03	2.97	3.94E-05	2.85	4.46E-04	2.61
	160	7.28E-06	3.06	1.35E-04	3.11	4.72E-06	3.06	6.74E-05	2.73

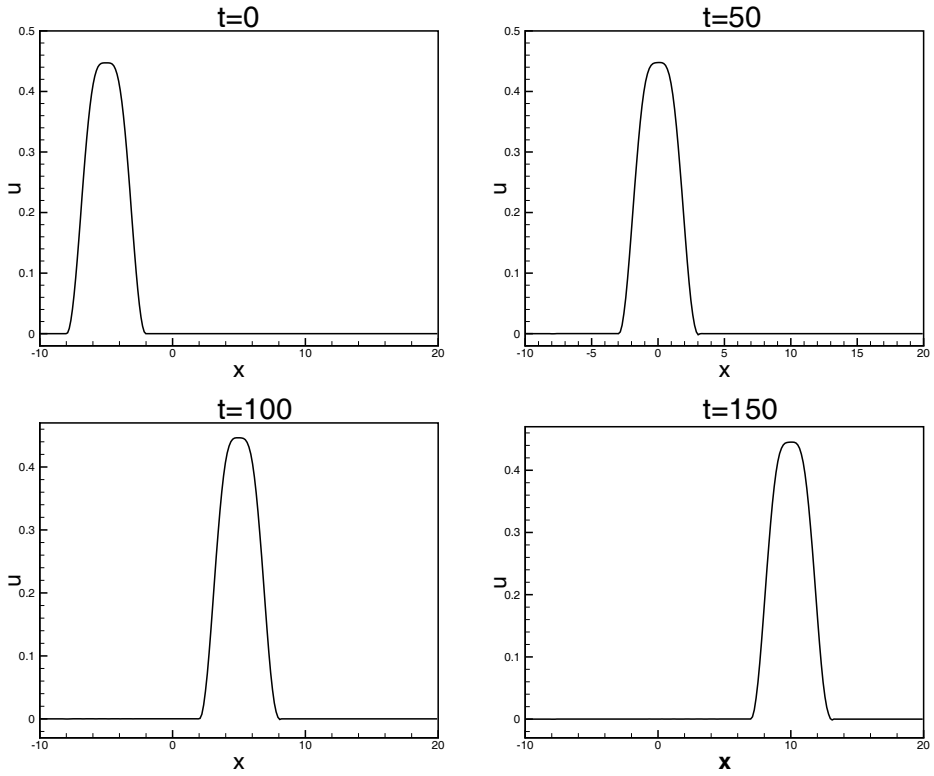

Figure 3.14: The single compacton. The initial data is taken as (3.28), where $\delta = 0.09$, $x_0 = -5$, $\lambda = 0.1$. Using P^1 elements with 220 cells in [-10,20].

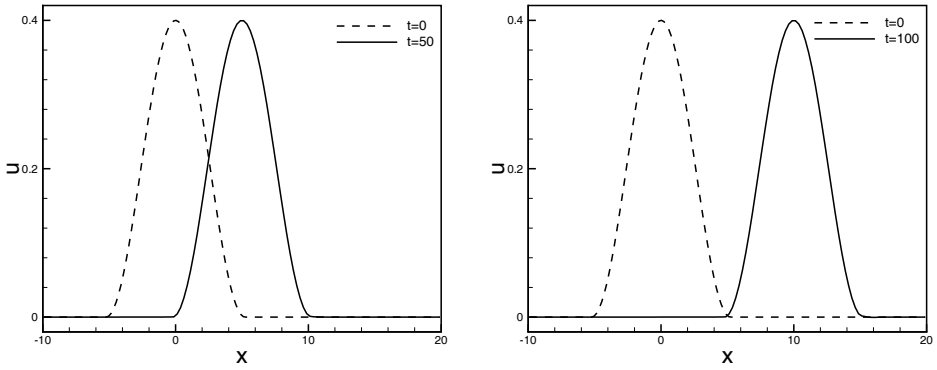

Figure 3.15: The single compacton solution of $K(3,3,3)$. The initial data is taken as (3.33) and (3.31), where $x_0 = 0$, $\lambda = 0.1$. Using P^2 elements with 120 cells in [-10,20].

Next, we show the single compacton propagation in Figure 3.15 for the initial condition

$$u(x,0) = \begin{cases} A\cos^{\delta}(B(x-x_0)) & |B(x-x_0)| \le \frac{\pi}{2} \\ 0 & \text{otherwise} \end{cases} \tag{3.33}$$

where δ, A and B are defined in (3.31) for $K(3,3,3)$.

4. Concluding Remarks

We have further developed the local discontinuous Galerkin method to solve three classes of general nonlinear wave equations formulated by the KdV-Burgers type equations, the fifth-order KdV type equations and the fully nonlinear $K(n, n, n)$ equations and have proven their stability. Numerical examples for nonlinear problems are shown to illustrate the accuracy and capability of the methods.

References

[1] F. Bassi and Rebay, A high-order accurate discontinuous finite element method for the numerical solution of the compressible Navier-Stokes equations, *J. Comput. Phys.,* **131** (1997), 267-279.

[2] D.J. Benney, Long waves on the liquid films, *J. Math. Phys.*, **45** (1966), 150-155.

[3] J.L. Bona, V.A. Dougalis, O.A. Karakashian and W.R. McKinney, Computations of blow-up and decay for periodic solutions of the generalized Korteweg-de Vries-Burgers equation, *Appl. Numer. Math.*, **10** (1992), 335-355.

[4] J.P. Boyd, Weakly non-local solitons for capillary-gravity waves: fifth-order Korteweg-de Vires equation, Physica D, **48** (1991), 129-146.

[5] J.P. Boyd, Numerical computations of a nearly singular nonlinear equation: Weakly nonlocal bound states of solitons for the fifth-order Korteweg-de Vires equation, *J. Comput. Phys.*, **124** (1996), 55-70.

[6] J. Canosa and J. Gazdag, The Korteweg-de Vires-Burgers equation, *J. Comput. Phys.*, **23** (1977), 393-403.

[7] B. Cockburn, Discontinuous Galerkin methods for methods for convection-dominated problems, in High-Order Methods for Computational Physics, T.J. Barth and H. Deconinck, editors, Lecture Notes in Computational Science and Engineering, volume 9, Springer, 1999, 69-224.

[8] B. Cockburn, S. Hou and C.-W. Shu, The Runge-Kutta local projection discontinuous Galerkin finite element method for conservation laws IV: the multidimensional case, *Math. Comp.*, **54** (1990), 545-581.

[9] B. Cockburn, G. Karniadakis and C.-W. Shu, The development of discontinuous Galerkin methods, in Discontinuous Galerkin Methods: Theory, Computation and Applications, B. Cockburn, G. Karniadakis and C.-W. Shu, editors, Lecture Notes in Computational Science and Engineering, volume 11, Springer, 2000, Part I: Overview, 3-50.

[10] B. Cockburn, S.-Y. Lin and C.-W. Shu, TVB Runge-Kutta local projection discontinuous Galerkin finite element method for conservation laws III: one dimensional systems, *J. Comput. Phys.*, **84** (1989), 90-113.

[11] B. Cockburn and C.-W. Shu, TVB Runge-Kutta local projection discontinuous Galerkin finite element method for conservation laws II: general framework, *Math. Comp.*, **52** (1989), 411-435.

[12] B. Cockburn and C.-W. Shu, The Runge-Kutta discontinuous Galerkin method for conservation laws V: multidimensional systems, *J. Comput. Phys.*, **141** (1998), 199-224.

[13] B. Cockburn and C.-W. Shu, The local discontinuous Galerkin method for time-dependent convection-diffusion systems, *SIAM J. Numer. Anal.*, **35** (1998), 2440-2463.

[14] B. Cockburn and C.-W. Shu, Runge-Kutta discontinuous Galerkin methods for convection-dominated problems, *J. Sci. Comp.*, **16** (2001), 173-261.

[15] F. Cooper, J.M Hyman and A. Khare, Compacton solutions in a class of generalized fifth-order Korteweg-de Vires equations, *Phys. Rev. E*, **64** (2001), 026608.

[16] B.Dey, Compacton solutions for a class of two parameter generalized odd-order Korteweg-de Vires equations, *Phys. Rev. E*, **57** (1998), 4733-4728.

[17] B. Dey, A. Khare and C.N. Kumar, Stationary solitons of the fifth order KdV-type. Equations and their stabilization, *Phys. Let. A*, **223** (1996), 449-452.

[18] H. Gard and P.N. Hu, Unified shock profiles in a plasma, *Phys. Fluids*, **15** (1967), 2596-2602.

[19] J.K. Hunter and J.M. Vanden-Broeck, Solitary and periodic gravity-capillary waves of finite amplitude, *J. Fluid Mech.*, **134** (1983), 205-219.

[20] J.K. Hunter and J. Scheurle, Existence of perturbed solitary wave solutions to a model equation for water waves, *Physica D*, **32** (1988), 253-268.

[21] J.M. Hyman and P. Rosenau, Pulsating multiplet solutions of quintic wave equations, *Physica D*, **123** (1999), 502-512.

[22] M. Ito, An extension of nonlinear evolution equation of the K-dV (mK-dV) type to high orders, *J. Phys. Soc. Japan*, **49** (1980), 771-778.

[23] T. Kawahara, Oscillatory solitary waves in dispersive media, *J. Phys. Soc. Japan,* **33** (1972), 260-265.

[24] D. Levy, C.-W. Shu and J. Yan, Local discontinuous Galerkin methods for nonlinear dispersive equations, *J. Comput. Phys.*, to appear.

[25] V.A. Marchenko, Long waves in shallow liquid under ice cover, *J. Appl. Math. Meth.*, **52** (1988), 180-183.

[26] P. Rosenau and D. Levy, Compactons in a class of nonlinearly quintic equations, *Phys. Let. A*, **252** (1999), 297-306.

[27] C.-W. Shu and S. Osher, Efficient implementation of essentially non-oscillatory shock-capturing schemes, *J. Comput. Phys.*, **77** (1988), 439-471.

[28] C.H. Su and C.S. Gardner, Korteweg-de Vires equation and generalizations. III. Derivation of the Korteweg-de Vires equation and Burgers equation, *J. Math. Phys.*, **10** (1969), 536-539.

[29] Y. Yamamoto and E.I. Takizawa, On a solution of nonlinear time -evolution equation of fifth order, *J. Phys. Soc. Japan*, **50** (1981), 1421-1422.

[30] J. Yan and C.-W. Shu, A local discontinuous Galerkin method for KdV type equations, *SIAM J. Numer. Anal.*, **40** (2002), 769-791.

[31] J. Yan and C.-W. Shu, Local discontinuous Galerkin methods for partial differential equations with higher order derivatives, *J. Sci. Comp.*, **17** (2002), 27-47.

[32] X. Zhong, Additive semi-implicit Runge-Kutta methods for computing high-speed nonequilibrium reactive flows, *J. Comput. Phys.*, **128** (1996), 19-31.

[33] S.I. Zaki, A quintic B-spline finite elements scheme for the KdVB equation, *Comput. Methods Appl. Mech. Engrg.*, **188** (2000), 121-134.